Electromechanical Response of Polycrystalline Barium Titanate Resolved at the Grain Scale

Majkut, Marta; Daniels, John E.; Wright, Jonathan P.; Schmidt, Søren; Oddershede, Jette

Published in:
Journal of the American Ceramic Society

Link to article, DOI:
10.1111/jace.14481

Publication date:
2017

Document Version
Publisher's PDF, also known as Version of record

J. Am. Ceram. Soc., 1–8 (2016)
DOI: 10.1111/jace.14481

journal

Electromechanical Response of Polycrystalline Barium Titanate Resolved at the Grain Scale

Marta Majkut,[‡] John E. Daniels,[§] Jonathan P. Wright,[¶] Søren Schmidt,[‡,†] and Jette Oddershede[‡,†]

[‡]Department of Physics, Technical University of Denmark, Fysikvej, 2800 Kgs. Lyngby, Denmark

[§]School of Materials Science and Engineering, UNSW Australia, Sydney, NSW 2052, Australia

[¶]European Synchrotron Radiation Facility, Grenoble 38000, France

Ferroic materials are critical components in many modern devices. Polycrystalline states of these materials dominate the market due to their cost effectiveness and ease of production. Studying the coupling of ferroic properties across grain boundaries and within clusters of grains is therefore critical for understanding bulk polycrystalline ferroic behavior. Here, three-dimensional X-ray diffraction is used to reconstruct a 3D grain map (grain orientations and neighborhoods) of a polycrystalline barium titanate sample and track the grain-scale non-180° ferroelectric domain switching strains of 139 individual grains *in situ* under an applied electric field. The map shows that each grain is located in a very unique local environment in terms of intergranular misorientations, leading to local strain heterogeneity in the as-processed state of the sample. While primarily dependent on the crystallographic orientation relative to the field directions, the response of individual grains is also heterogeneous. These unique experimental results are of critical importance both when building the starting conditions and considering the validity of grain-scale modeling efforts, and provide additional considerations in the design of novel ferroic materials.

Keywords: *X-ray methods; polycrystalline materials; microstructure; domains*

I. Introduction

Ferroic materials showing switchable order parameters under an external stimulus are key components in many modern devices. An example is electromechanical materials that directly couple mechanical stress with electrical charge via the piezoelectric effect and are used for actuation applications.[1] Lead–zirconate–titanate (PZT)-based piezoelectric ceramics dominate industrial applications, primarily due to the combination of large piezoelectric coefficients and good temperature stability. Ceramics are also easier to manufacture and more cost-effective than single crystals. Recent regulations in North America, Europe, and elsewhere are pushing for lead-free alternatives,[2,3] leading to the discovery of some high-performance lead-free piezoceramics and reinvigorating studies into the fundamental nature of electromechanical coupling.

Barium titanate (BT) is a prototypical perovskite piezoelectric material and was one of the first piezoceramics discovered. It is readily produced in ceramic form and is commonly used as an end-member component of many disordered perovskites that have been identified as potential high-performance lead-free piezoelectrics.[4–9] Above the Curie temperature, T_C, of roughly 130°C, BT is in the paraelectric cubic phase, transforming to a ferroelectric tetragonal phase upon cooling through T_C. Since any of the primary cubic directions may become the anisotropic tetragonal *c*-axis, the transformation results in a domain structure within each grain, composed of both 180° and non-180° domains. The domains form such that the total energy of the system (e.g., elastic, electrical, etc.) is minimized, resulting in complex microstructures across many length scales.[10,11] Additionally, due to the anisotropic thermal expansion coefficient, the interlocked, differently oriented grains develop thermal stresses during cooling. This results in a spatially distributed, built-in electric field in the as-processed ceramic, generated via the direct piezoelectric effect. The magnitude of this electric field is maximum at grain boundaries and corners, where the stresses are largest.[12]

Non-180° domain wall motion represents a significant contribution to the overall strain response of piezoceramics. Powder diffraction studies[1,13–15] have demonstrated that, on average, domain switching behavior depends on grain orientation, with the polarization tending to align as closely with the electric field direction as allowed by the crystallite orientation. This has made texture a very important topic with regard to engineering lead-free piezoceramics with properties approaching those of their PZT counterparts.[16,17] It is clear, however, that it is not just the grain orientation that plays a role in domain switching. Simulations reveal that domain switching tends to initiate at grain boundaries and corners, where stress concentrations exist.[12] Surface measurements by piezoresponse force microscopy reveal large deviations in the hysteresis loops of adjacent grains, with the effect again most pronounced at the grain boundaries.[18] It has been suggested that there may exist characteristic grain boundaries that serve to either enhance or inhibit domain switching and strain response.[19,20] Domains have also been observed crossing grain boundaries, suggesting the possibility of longer range coupling.[21]

Such correlated mesoscale phenomena have often proven difficult to study, and benefit greatly from a combination of modeling and imaging techniques.[17,22–24] Powder diffraction studies give insight into the average mechanics, while grain-scale information revealed by imaging techniques is generally limited to two-dimensional surface measurements. Simulations and modeling offer an opportunity for in-depth investigation of length scales that are inaccessible experimentally. Phase field models have in particular contributed to the understanding of domain structures under an electrical field.[25–27] However, models require experimental input for validation, typically macroscopic measurements such as texture, piezoelectric constants, and hysteresis loops. It is

J. Ihlefeld—contributing editor

Manuscript No. 38631. Received May 23, 2016; approved August 3, 2016.
[†]Authors to whom correspondence should be addressed. e-mails: ssch@fysik.dtu.dk and jeto@fysik.dtu.dk

important to consider that a model in macroscopic agreement with experiment may not always capture local effects, as demonstrated by comparisons between self-consistent models, where the grain interaction is smoothed, and finite element models, where the grain interaction is preserved.[28]

In this work, we present a three-dimensional microstructure measurement where the grain morphology, orientation, and neighborhood of a coarse-grained BT sample is reconstructed. Domain volume fractions of the three crystallographically unique tetragonal non-180° domain variants are extracted for individual grains and used to calculate the grain-scale non-180° domain switching strains in the as-processed state of the ceramic, as well as under the stimulus of an externally applied electric field. The data are measured using a combination of near-field and far-field three-dimensional X-ray diffraction (3DXRD). We present results regarding the effect of microstructural grain features on the grain-scale ferroelastic switching strain. Additionally, we discuss the possible use of this unique dataset for polycrystal model input and validation. Such integrated experimental and modeling approaches have previously been used to study, for example, deformation twinning in hexagonal close-packed metals.[29–31] Three-dimensional experimental data have been identified as key for the direct validation of computational materials science approaches[32,33] that are becoming increasingly important for both academia and industry.

II. Experimental Procedure

BT ceramic was prepared with a grain size of approximately 50–70 μm and cut and polished into a cuboid sample of dimensions 300 μm × 300 μm × 400 μm. The sample was mounted in a setup that allows application of a high electrical field with minimal risk of dielectric breakdown (additional details can be found in Daniels et al.[34]).

The 3DXRD experiments were performed at beamline ID11 of the European Synchrotron Radiation Facility (ESRF). For the far-field experiment, which yields domain volume fraction and strain information, the beam was focused to a planar geometry of height 100 μm, illuminating the entire width of the specimen, with an energy of 78.395 keV (Pt edge). The sample was mounted 485 mm away from the Frelon4M detector (ESRF, Grenoble, France)[35] with 2048 × 2048 pixels of 50 μm × 50 μm and diffraction images were collected while rotating the sample in the angular range of 345° about the vertical z-axis in steps of 0.1°. Three adjacent 100 μm layers of the sample were mapped in the as-processed state (F0), at an intermediate electric field strength close to the coercive field (F1) and at a field exceeding the coercive field (F2), with the electric field direction coincident with the rotational z-axis.

For the subsequent near-field experiment, which yields a grain map of the 3D microstructure, an X-ray beam energy of 37.010 keV (just below the Ba K-edge) was used. The beam dimensions were limited to 500 μm horizontally and 100 μm vertically with lenses and slits. Again three adjacent 100 μm layers of the sample were mapped through 360° in steps of 0.1° for the first layer and 0.2° for the remaining two. Near-field mapping employs two detectors simultaneously: the Frelon4M detector mentioned previously at a distance of 223 mm and the first screen of the Risø 3D-detector (DTU, Roskilde, Denmark)[36] with 2048 × 2048 pixels of 1.4 μm × 1.4 μm at a distance of 8 mm.

The collected diffraction image stacks were analyzed using the Fable software suite (2014) (ESRF and DTU), described in detail in Sørensen et al.[37] The individual grains were indexed from the far-field data using GrainSpotter,[38] and the indexed grain orientations were then used as seeds for the reconstruction of a grain map from the near-field data by means of a 3D generalization of GrainSweeper.[39] For each 2 μm × 2 μm ×2 μm voxel in the reconstruction, the seed orientation with the highest completeness ratio of expected to observed number of reflections was assigned. The three adjacent reconstructed layers were stacked along the z-axis—the common poling and rotation axis—in order to obtain the 3D orientation map, and voxels with completeness less than 60% were eliminated from the map. The orientation map was then registered to a grain map by assigning adjacent voxels with pseudocubic misorientations less than 1° to the same grain. Finally, microstructural information, such as grain neighbors, were extracted from the grain map using DREAM.3D (BlueQuartz Software, Springboro, OH).[40]

One hundred sixty-five unique grains were indexed from the far-field data measured at F0, F1, and F2 using Fable (2014) and GrainSpotter,[38] resulting in a list of their orientations and 3D positions, as well as a list of diffraction spots assigned to each grain. The (200)/(002) peaks of these grains were then extracted from the data since these peaks contain the information about the volume fractions, v_{200}, v_{020}, and v_{002}, of the three unique ferroelastic domain variants, d_{200}, d_{020}, and d_{002}, distinguishable with the current method. Each reflection was integrated along the rotation, ω, and the azimuth, η, yielding a radial profile along 2θ, which was then fit with Gaussian peaks centered at the split peak positions $2\theta_{min}$ and $2\theta_{max}$, as shown for a single grain at F0 and F2 in Fig. 1(a).

If a portion of the grain falls outside of the illuminated volume, the measured peak intensities may no longer be representative of the true domain volume fractions (e.g., if the unilluminated part of the grain contains many domains of the d_{002} variant), hence grains of this type were excluded from further analysis. After this procedure, domain volume fractions were fit based on the intensity ratios of the (200)/(002) reflections and error bars were estimated as outlined by Oddershede et al.[41] for 139 embedded grains.

The non-180° domain switching strain resolved along the poling direction, ε_p, was then calculated from the extracted domain volume fractions along the unit vector l as[42]:

$$\varepsilon_p = \left(\frac{c-a}{a_0}\right)\left(v_{200}l_1^2 + v_{020}l_2^2 + v_{002}l_3^2 - \frac{1}{3}\right) \quad (1)$$

where c and a are the tetragonal lattice parameters and, without an independent measure of the cubic lattice parameter, $a_0 = \sqrt[3]{ca^2}$, which assumes that there is no volume change at T_C. For l = <111> or $v_{200} = v_{020} = v_{002} = 1/3$ the strain $\varepsilon_p = 0$ because $v_{200} + v_{020} + v_{002} = 1$ and $l_1^2 + l_2^2 + l_3^2 = 1$. The maximum poling strain of $2(c-a)/3a_0$ is obtained for a single domain with <100> aligned along the electric field direction, while the minimum is $(a-c)/3a_0$. Propagation of error bars on v_{200}, v_{020} and v_{002} to an error bar on ε_p was performed.[41]

The relationship between the domain volume fractions and ε_p is demonstrated in Fig. 1(b), where the bars are divided into three parts representing the volume fraction of each of the three non-180° ferroelastic domains, labeled with the domain c-axis misorientation with the poling direction, and the line is ε_p. The applied electric field results in the expected increase of ε_p, from $-0.126\% \pm 0.003\%$ at F0 to $0.492\% \pm 0.014\%$ at F2, a direct result of the growth of d_{002} at the expense of d_{200} and d_{020}. This change is again evident in the shifting of intensity from relatively even ratios at F0 to a very strong peak at F2 [Fig. 1(a)]. The dominant growth of d_{002} is expected since it is by far the most favorably aligned with respect to the electric field vector at a misorientation of 10.5° [see inset in Fig. 1(b)].

III. Results and Discussion

(1) The Effect of Thermal Stresses in the As-Processed State

Figure 2 shows the distribution of non-180° domain switching strains for all grains at F0. While the strains

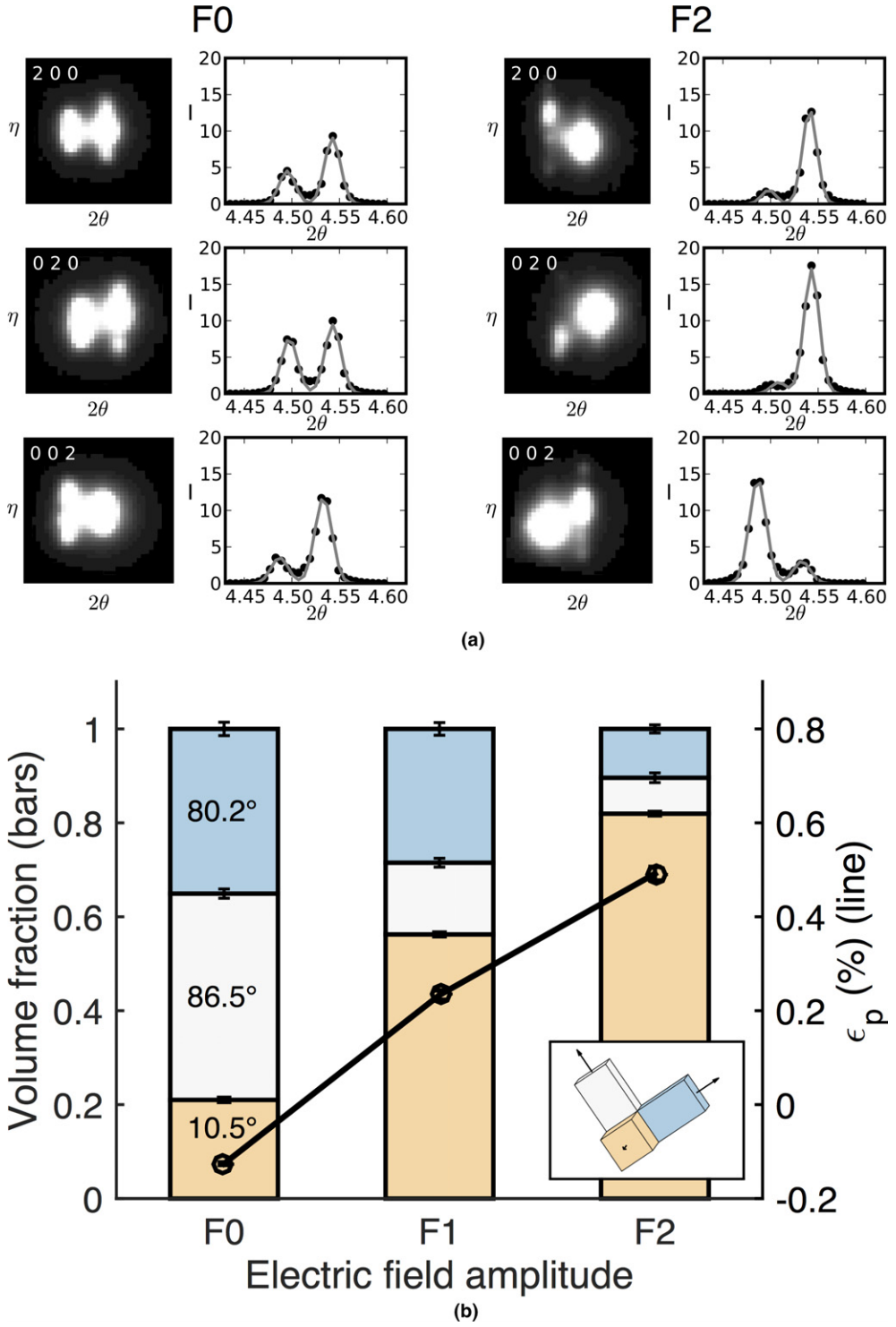

Fig. 1. For the same [001]-oriented grain (a) the typical raw and integrated (200)/(002) diffraction spots at the initial (F0) and final (F2) electric fields, and (b) the change in volume fraction of domains (bars) with poling and the corresponding non-180° domain switching strain along the poling direction (line). Each segment of the bar represents a domain within the grain of interest and is labeled with the misorientation between the domain *c*-axis and the applied field direction as illustrated in the inset (field direction out of the plane).

within the polycrystal balance and the mean volume weighted strain of the sample as a whole is $\varepsilon_{p,F0} = -0.002\% \pm 0.001\%$, the as-processed strain state of the sample is heterogeneous at the grain scale and individual grains do not contain equal volume fractions of the three possible ferroelastic domain variants [which would yield $\varepsilon_p = 0$ from Eq. (1)]. These observations are consistent with recent micromechanical modeling of related ferroelectric/ferroelastic materials, which show a large spread in intergranular residual stresses even when no field is applied and the average internal stress is zero.[43]

Heterogeneity in the grain-scale domain volume fractions is expected to result from the anisotropic thermal expansion coefficients of tetragonal BT, and is consistent with simulation results that show a built-in, spatially distributed polarization in the as-processed state.[12] The resultant anisotropic ferroelastic strain must inevitably induce large elastic compliance strains at the grain scale to compensate, as observed in powder diffraction studies.[1] Additionally, the electrostatic energy associated with ferroelectric domain interactions at grain boundaries must outweigh the increased elastic energy caused by the strain heterogeneity.[25]

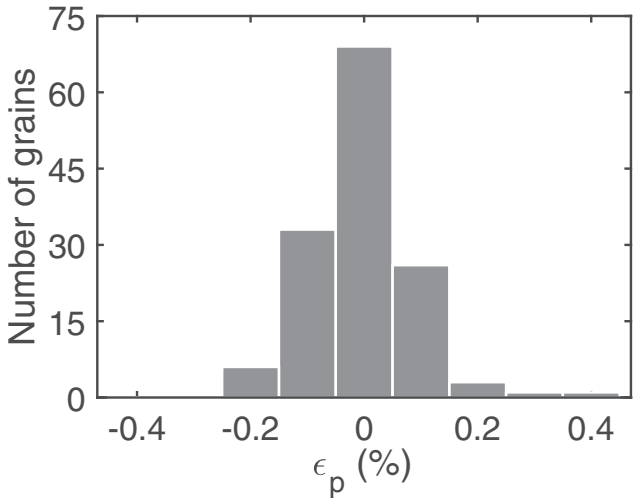

Fig. 2. Distribution of non-180° domain switching strains in the initial as-processed state of the barium titanate sample. The distribution width is an indicator of the grain-scale strain heterogeneity in the as-processed state.

In the present dataset, there is even evidence of such local intragranular lattice strains. For instance, all the raw data in Fig. 1(a) have more intensity between the two peaks corresponding to $2\theta_{min}$ and $2\theta_{max}$ than justified by the combined tails of the peaks, indicating a lattice strain distribution within the domains that tends toward the common pseudocubic orientation of the domains. This scattering has been speculated to result from strain compatibility at the domain boundaries.[44]

(2) Strain Response Heterogeneity

The inverse pole figure in Fig. 3(a) shows that the grains are randomly oriented, as expected for the ceramic processing technique used, a result also confirmed by a Mackenzie type analysis.[45] The color represents the difference in non-180° domain switching strain between the F0 and F2 states, from here on termed the ferroelastic strain response. From Fig. 3(a) it is clear that there is a general trend toward maximum and minimum ferroelastic strain response occurring at grain orientations with a <100> and <111> direction lying close to the electric field vector, respectively, as expected from the definition of ε_p in Eq. (1) as well as from previous powder diffraction results.[1,13–15] However, in addition to the observed first-order correlation between grain orientation and ferroelastic strain response there are significant variations, or second-order perturbations, within groups of grains with similar orientations. To highlight these variations, Fig. 3(b) shows the ferroelastic strain response as a function of $\cos^2\phi_{100}$, where ϕ_{100} is the misorientation between the electric field vector and the closest <100> direction in the given grain. Although it would be reasonable to think that grains with an initially negative strain would have more potential for domain switching and thus a larger ferroelastic strain response, as suggested by finite element studies[46], the magnitude of initial ferroelastic strain, $\varepsilon_{p,F0}$, in a grain did not show any correlation with the response under high electric field.

The present experimental results show that while, at the bulk level, the ferroelastic strain response is as expected, i.e., zero at the initial state before increasing upon application of an electric field ($\varepsilon_{p,F1} = 0.088\% \pm 0.001\%$ and $\varepsilon_{p,F2} = 0.135\% \pm 0.001\%$), the ferroelastic strain response is heterogeneous at the grain scale. To study the effect of grain response averaging, the RMS distance to the trend line in Fig. 3(b) was calculated for an average over a group of grains of similar orientation at a variety of group sizes. It

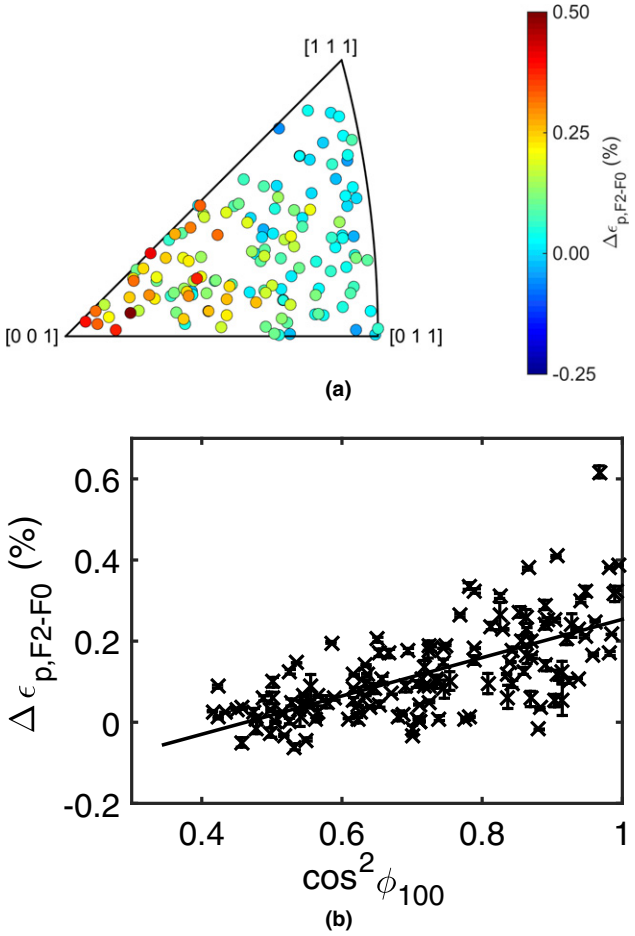

Fig. 3. (a) The orientation of the 139 indexed grains color coded according to the ferroelastic strain response from step F0 to F2, and (b) $\varepsilon_{p,F2}-\varepsilon_{p,F0}$ as a function of $\cos^2\phi_{100}$, where ϕ_{100} is the misorientation between the electric field vector and the closest <100> direction in the given grain. The trend line in (b) corresponds to the average behavior expected for a given grain orientation.

was found that the RMS distance was halved for groups of 10 similarly oriented grains as compared to individual grains, which agrees well with our previous measurements of grain-scale heterogeneity.[47] The present work builds on this by combining the domain volume-fraction information with the 3D microstructure grain map, reconstructed from the near-field data and shown in Fig. 4, where individual grains are colored by the non-180° domain switching strains at (a) $\varepsilon_{p,F0}$ and (b) $\varepsilon_{p,F2}$, extracted from far-field data. The combination of these two results enables a correlative study of ferroelastic strain response with microstructural features of the grains themselves as well as their local neighborhoods.

Figure 5(a) shows the effect of grain size on ferroelastic strain response relative to the trend line in Fig. 3(b). The grain diameter here is calculated from the volumes derived from the grain map by assuming that the grains are spheres. The calculated correlation coefficient of 0.1 indicates no significant correlation between grain diameter and ferroelastic strain response. While previous experiments[48] and simulations[26] have demonstrated the effect of average sample grain size on domain switching behavior and material response, this effect does not appear to be present at the individual grain level of the current coarse-grained sample, consistent with the fact that scaling effects become significant only at grain sizes below 10 μm.[49]

It is well-known that the boundary conditions experienced by a grain at the surface of the sample are different from those of a grain in the bulk.[26,42] To investigate how this is reflected in the current experimental results, the distribution

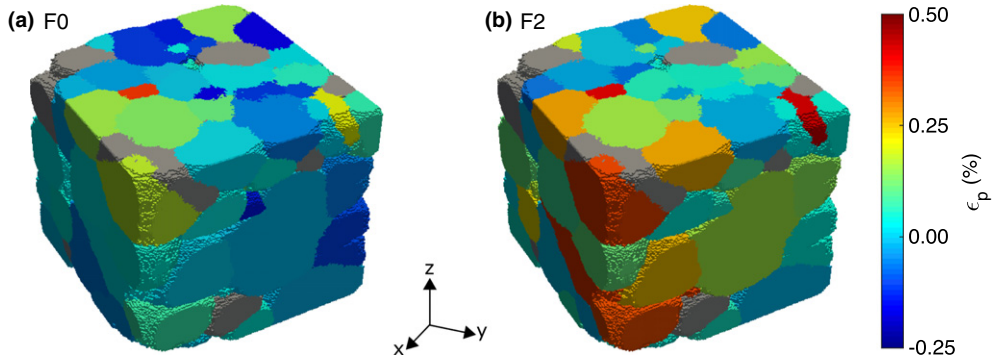

Fig. 4. Grain maps of the entire sample color coded according to (a) $\varepsilon_{p,F0}$, and (b) $\varepsilon_{p,F2}$. The poling direction is along the vertical z-axis. The gray grains are the ones where the fit of domain volume fractions failed, primarily grains on the top and bottom surfaces that were removed from the analysis because they extend beyond the illuminated volume.

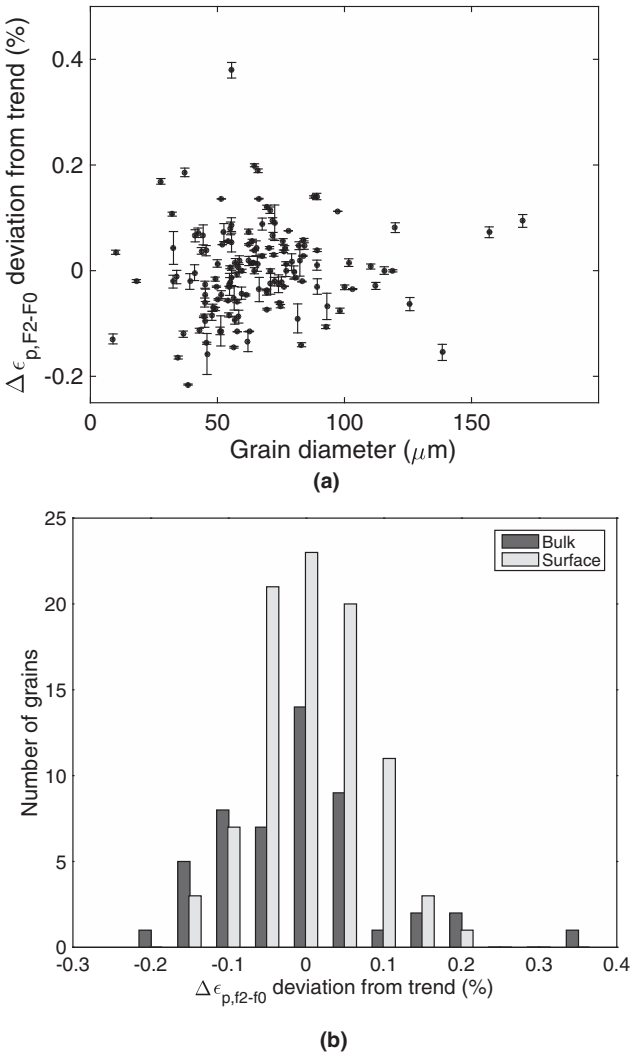

Fig. 5. (a) Ferroelastic strain response difference from average behavior as a function of grain diameter, and (b) distribution of ferroelastic strain responses away from average behavior for the 50 bulk grains (dark) and 89 surface grains (light).

of ferroelastic strain response deviation from the trend line is shown in Fig. 5(b) for the 50 bulk grains (dark) and 89 surface grains (light) in the sampled volume. The average of the bulk distribution is −0.01% with an absolute spread of 0.11%, while the average and absolute spread for the surface grains are 0.01% and 0.07%, respectively. This implies that there is no significant difference between bulk and surface grains in terms of their mean deviation from the linear trend, however, the spread of response magnitude in the surface grains is significantly lower than for bulk grains, with the probability of equal spread in the two distributions calculated as 0.06% for all data points and 3% for data points within the range of ±0.2% from the trend line. A more homogeneous response is expected for surface grains since they experience fewer constraints due to the relaxed elastic and electrostatic boundary conditions at the sample surface.[50]

The grain size and location in the sample are also intimately linked with the number of contact neighbors that a grain has, i.e., small/surface grains generally have fewer neighbors than large/bulk grains. However, the correlation coefficient between the ferroelastic strain response away from the trend line and the number of neighbors is merely 0.02, hence it is concluded that neither the grain diameter nor number of neighbors nor the location of grains within the sample have any significant effect on the ferroelastic strain response of individual bulk grains within the polycrystalline BT sample.

(3) Effects of the Grain Neighborhood

In order to experimentally assess the effects of grain interactions, two bulk grains, A and B, have been selected for further analysis. Some of their properties and those of their neighbors have been summarized in Table I. The grains were chosen specifically to be of similar orientation relative to the electric field vector ($5° < \phi_{100} < 15°$ for both) and similar size (both have grain diameters slightly smaller than the sample average of 64 μm), yet exhibiting significantly different ferroelastic strain responses. Grain A, which was used as an example in Fig. 1, experiences a relatively large ferroelastic strain response, while grain B experiences a ferroelastic strain response approximately equal to the average of all grains of similar orientation.

The local environments of grains A and B and their neighbors, shown in Fig. 6, have been analyzed in detail in order to quantify various aspects of the grain neighborhoods. Both grains have a similar number of neighbors, 10 for A and 14 for B. This is comparable to the average number of 11 neighbors per grain in the sample. The neighbors of grain A are on average larger than those of grain B, which is expected considering the similar grain diameters of A and B and the difference in number of neighbors. However, this average does not make clear that grain A has two very large neighbors (diameters 157 and 170 μm), while the largest neighbor of grain B has a diameter of only 125 μm.

The Mackenzie plot in Fig. 7(a), generated for all neighboring grain pairs in the sample, shows that for a random grain in the polycrystalline BT sample it is statistically likely that the grain is surrounded by neighbors that come very close to the average random texture of the entire sample.

Table I. Properties of the Two Selected Grains A and B

	Grain A	Grain B
ϕ_{100} (°)	10.5°	7.12°
Grain diameter (μm)	56	55
$\varepsilon_{p,F2}-\varepsilon_{p,F0}$ (%)	0.617 ± 0.015	0.217 ± 0.002
Volume fraction switched from F0 to F2	0.61	0.21
Number of neighbors	10	14
Neighbor diameter (μm)		
Average	84	63
Spread	44	28
Neighbor ϕ_{100} (°)		
Average	36	43
Spread	15	25
Neighbor misorientation (°)		
Average	40	32
Spread	8	12

For the neighbor diameters, neighbor orientation relative the poling direction (ϕ_{100}) and neighbor misorientation relative to the grains in question, both the average and spread of the distribution over all neighbors for grains A and B are given.

However, Fig. 7(b) showing the distributions of neighbor misorientations for grains A (dark) and B (light), clearly demonstrate that in reality an individual grain sees a local neighborhood that is significantly different from the statistical average, as also indicated by the mean and spread of the two distributions given in Table I. So, while the bulk macroscopic properties and response are predictable, at the grain-scale the material behavior is far more localized in nature, as has been predicted from multigrain models and simulations.[51,52]

Figure 6 also indicates that it is not only grain A that has a larger strain response than B, but so does its immediate neighborhood as a whole. A reason could be that grains in the neighborhood of grain A are generally more favorably aligned relative to the field vector. Another possible explanation could be the presence of the so-called Σ3 boundaries with neighbor misorientations close to 60° that have been suggested to play a special role in connection with continuity of ferroelectric domain structures across grain boundaries.[19,20] However, neither A nor B exhibit any such neighbor misorientations.

The two grains are not representative of the sample texture as a whole, but rather selected to represent extremes of the response distribution caused by intergranular interactions. Consideration of such local environments is essential for predicting the local maximum stresses that are important for the reproducibility and reliability of the ferroelectric response in a ceramic.[17,28,51] Depending on the actuation mechanisms within a specific ceramic material, the stress concentrations may vary significantly due to the degree of strain anisotropy. In cases where large intergranular stresses exist, these may accelerate the initiation of cracks that lead to fatigue and failure of the material.[53]

We note that the spatial resolution of the current experimental results does not enable a distinction between individual domains within grains, only the domain volume fractions. Hence, a direct comparison between experiment and model is best performed for models not concerned with the specific domain structure. In particular, crystal plasticity-based finite elements models, where the incremental transformation by domain wall motion is analogous to incremental slip on a slip system for deformation studies, would greatly benefit from the present data both for input and validation purposes. There the state of the sample is described by the volume fractions of each domain type,[54] making the modeling results directly comparable with their experimental counterparts.

Previous modeling attempts have considered the effect of grain orientation, assuming that all grains are of equal size with all domains of equal volume fraction in either 2D[28,46,51] or 3D,[55] while the present study has clearly demonstrated that this is not the case. The first 3D simulation of faceted grains of variable size (made by Voronoi tessellation from a random texture) represents an important step toward modeling real structures.[56] In some cases, real 3D microstructures measured by serial sectioning and EBSD have been used as input,[17] however, it is most often the case that microstructural input relies on simulation and extrapolation of selected grain morphology and orientation measurements.[12,28,46,51,52,55–57]

Macroscopic measurements such as hysteresis loops and piezoelectric constants are often used for validation. While these are useful measures, it has been shown that such macroscopic measurements can agree without the model capturing the local interactions that are life limiting for the component.[28] The dataset presented in this work is a reconstruction of a real, three-dimensional sample, where the domain volume fractions of individual bulk grains can be tracked from the initial state and with subsequent application of an electric field. Using the microstructure as direct input to finite element or other simulations, models can be validated on the grain scale, in addition to macroscopic measurements.

IV. Conclusions

Using 3DXRD grain mapping, the grain-scale domain volume fractions in 139 grains of a BT ceramic were successfully extracted, and from this information the ferroelastic strain response of each grain was derived. In agreement with previous experiments (i.e., powder diffraction), it was found that tetragonal domains with *c*-axes more closely aligned with the poling direction ([001] aligned grains) tend to grow with the application of an electric field, thus resulting in larger ferroelastic strain responses. Although the average ferroelastic strain response of the sample was as expected, large

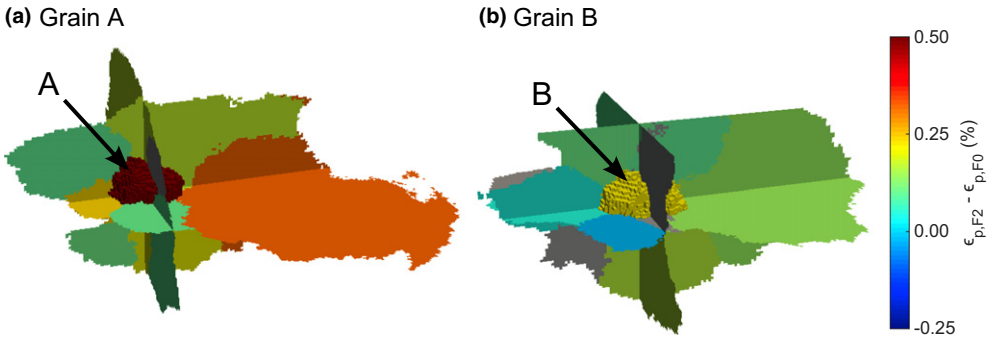

Fig. 6. Cutouts of the grain map showing grains A and B and their respective neighbors color coded according to the ferroelastic strain response of each grain, $\varepsilon_{p,F2}-\varepsilon_{p,F0}$. No strain information was fit for the gray neighbor grains, but their sizes and orientations are known.

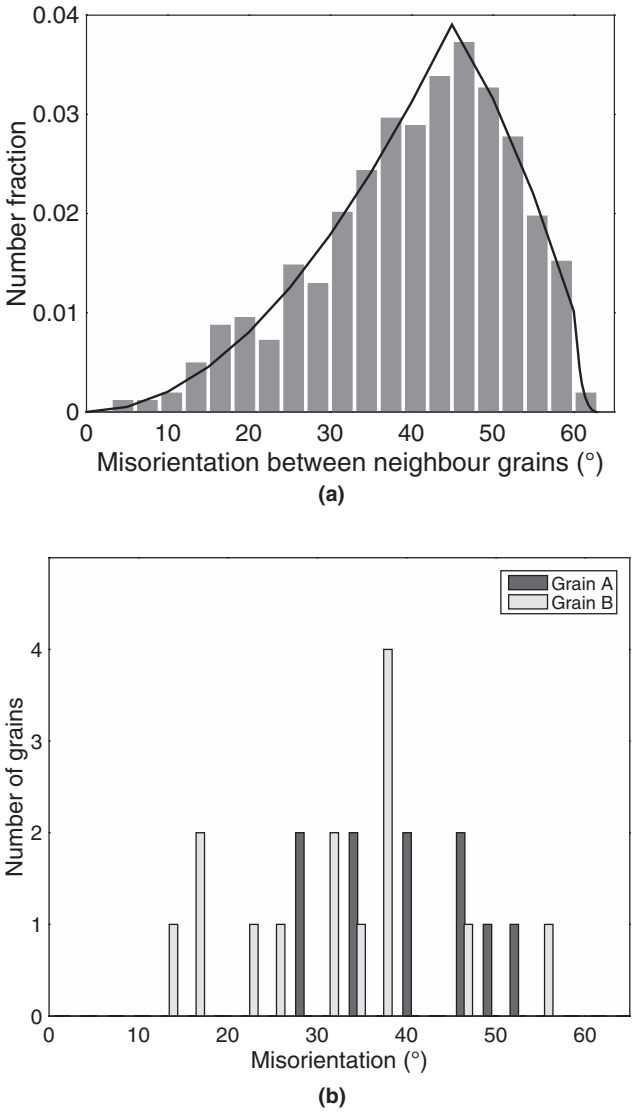

Fig. 7. Mackenzie type plot (a) for all misorientations of neighboring grains within the sample volume and the theoretical distribution of random orientations (line), and (b) neighbor misorientation distribution for grain A (dark) and grain B (light). All misorientations are calculated as the minimum rotation angle around an arbitrary axis needed to make the crystal lattice of a grain coincide with the crystal lattice of each of its neighbors.

variations exist in the behavior of individual grains of similar orientations. An important observation is that these variations are not restricted to the ferroelastic strain response, they were in fact observed already in the initial as-processed state of the sample. It is suggested that these grain-scale variations arise from local strain and electrostatic neighborhoods being highly heterogeneous within the bulk polycrystal. The neighborhood heterogeneities were clearly demonstrated from the grain map for two selected bulk grains of similar orientation, size and number of neighbors that were found to exhibit very different ferroelastic strain responses. In addition, the diffraction data showed evidence of substantial lattice strains within domains, probably mainly in the grain-boundary regions to accommodate the transition between domains and ensure stress equilibrium. All of these results suggest that the minimization of electrostatic potentials at the grain boundaries due to interacting ferroelectric domains is the cause of the observed grain-scale strain heterogeneities both in the as-processed state of the sample and when an electrical field is applied. These results are of critical importance both when building the starting conditions and considering the validity of grain-scale modeling efforts, and provide additional considerations in the design of novel electromechanical materials.

Acknowledgments

The authors acknowledge support from the Danish Independent Research Council | Technology and Production Sciences case no. 12-127449 and Australian Research Council Discovery Project DP 120103968. MM and JO acknowledge the Danish Agency for Science, Technology and Innovation for covering expenses in relation to the synchrotron experiment (through Danscatt). JED acknowledges support from an Australian Institute of Nuclear Science and Engineering research fellowship and travel funding provided by the International Synchrotron Access Program (ISAP) managed by the Australian Synchrotron and funded by the Australian Government. The European Synchrotron Radiation Facility is acknowledged for the provision of beam time.

References

[1]A. Pramanick, D. Damjanovic, J. E. Daniels, J. C. Nino, and J. L. Jones, "Origins of Electro-Mechanical Coupling in Polycrystalline Ferroelectrics During Subcoercive Electrical Loading," *J. Am. Ceram. Soc.*, **94** [2] 293–309 (2011).

[2]J. Rödel, W. Jo, K. T. P. Seifert, E.-M. Anton, and T. Granzow, "Perspective on the Development of Lead-Free Piezoceramics," *J. Am. Ceram. Soc.*, **92** [6] 1153–77 (2009).

[3]J. Rödel, K. G. Webber, R. Dittmer, W. Jo, and M. Kimura, "Transferring Lead-Free Piezoelectric Ceramics Into Application," *J. Eur. Ceram. Soc.*, **35** [6] 1659–81 (2015).

[4]T. Takenaka, K. Maruyama, and K. Sakata, "$(Bi_{1/2}Na_{1/2})TiO_3$–$BaTiO_3$ System for Lead-Free Piezoeletric Ceramics," *Jpn. J. Appl. Phys.*, **30** [9B] 2236–9 (1991).

[5]H. Nagata, M. Yoshida, Y. Makiuchi, and T. Takenaka, "Large Piezoelectric Constant and High Curie Temperature of Lead-Free Piezoelectric Ceramic Ternary System Based on Bismuth Sodium Titanate-Bismuth Potassium Titanate- Barium Titanate Near the Morphotropic Phase Boundary," *Jpn. J. Appl. Phys.*, **42**, 7401–3 (2003).

[6]Y. Makiuchi, R. Aoyagi, Y. Hiruma, H. Nagata, and T. Takenaka, "$(Bi_{1/2}Na_{1/2})TiO_3$–$(Bi_{1/2}K_{1/2})TiO_3$–$BaTiO_3$-Based Lead-Free Piezoelectric Ceramics," *Jpn. J. Appl. Phys.*, **44** [6B] 4350–3 (2005).

[7]J. Shieh, K. C. Wu, and C. S. Chen, "Switching Characteristics of MPB Compositions of $(Bi_{0.5}Na_{0.5})TiO_3$–$BaTiO_3$–$(Bi_{0.5}K_{0.5})TiO_3$ Lead-Free Ferroelectric Ceramics," *Acta. Mater.*, **55**, 3081–7 (2007).

[8]T. R. Shrout and S. J. Zhang, "Lead-Free Piezoelectric Ceramics: Alternatives for PZT?," *J. Electroceramics*, **19**, 111–24 (2007).

[9]S.-T. Zhang, A. B. Kounga, E. Aulbach, H. Ehrenberg, and J. Rödel, "Giant Strain in Lead-Free Piezoceramics $Bi_{0.5}Na_{0.5}TiO_3$–$BaTiO_3$–$K_{0.5}Na_{0.5}NbO_3$ System," *Appl. Phys. Lett.*, **91** [11] 112906, 3pp (2007).

[10]G. Arlt and P. Sasko, "Domain Configuration and Equilibrium Size of Domains in $BaTiO_3$ Ceramics," *J. Appl. Phys.*, **51** [9] 4956–60 (1980).

[11]G. Arlt, "Twinning in Ferroelectric and Ferroelastic Ceramics: Stress Relief," *J. Mater. Sci.*, **25**, 2655–66 (1990).

[12]E.-M. Anton, R. E. García, T. S. Key, J. E. Blendell, and K. J. Bowman, "Domain Switching Mechanisms in Polycrystalline Ferroelectrics With Asymmetric Hysteretic Behavior," *J. Appl. Phys.*, **105** [2] 024107, 8pp (2009).

[13]M. J. Hoffmann, M. Hammer, A. Endriss, and D. C. Lupascu, "Correlation Between Microstructure, Strain Behavior, and Acoustic Emission of Soft PZT Ceramics," *Acta. Mater.*, **49** [7] 1301–10 (2001).

[14]G. Tutuncu, M. Motahari, M. R. Daymond, and E. Ustundag, "A Modified Rietveld Method to Model Highly Anisotropic Ceramics," *Acta. Mater.*, **60** [4] 1494–502 (2012).

[15]R. C. Rogan, E. Üstündag, B. Clausen, and M. R. Daymond, "Texture and Strain Analysis of the Ferroelastic Behavior of $Pb(Zr,Ti)O_3$ by *In Situ* Neutron Diffraction," *J. Appl. Phys.*, **93** [7] 4104–11 (2003).

[16]Y. Saito, H. Takao, T. Tani, T. Nonoyama, K. Takatori, et al., "Lead-Free Piezoceramics," *Nature*, **432** [November] 1–4 (2004).

[17]S. B. Lee, T. S. Key, Z. Liang, R. E. García, S. Wang, et al., "Microstructure Design of Lead-Free Piezoelectric Ceramics," *J. Eur. Ceram. Soc.*, **33** [2] 313–26 (2013).

[18]R. Nath, R. E. García, J. E. Blendell, and B. D. Huey, "The Influence of Grain Boundaries and Texture on Ferroelectric Domain Hysteresis," *JOM*, **59** [1] 17–21 (2007).

[19]F. Ernst, M. L. Mulvihill, O. Kienzle, and M. Rühle, "Preferred Grain Orientation Relationships in Sintered Perovskite Ceramics," *J. Am. Ceram. Soc.*, **84** [8] 1885–90 (2001).

[20]S. Tsurekawa, K. Ibaraki, K. Kawahara, and T. Watanabe, "The Continuity of Ferroelectric Domains at Grain Boundaries in Lead Zirconate Titanate," *Scr. Mater.*, **56** [7] 577–80 (2007).

[21]Y. Ivry, D. Chu, J. F. Scott, and C. Durkan, "Domains Beyond the Grain Boundary," *Adv. Funct. Mater.*, **21** [10] 1827–32 (2011).

[22]J. Y. Li, R. C. Rogan, E. Üstündag, and K. Bhattacharya, "Domain Switching in Polycrystalline Ferroelectric Ceramics," *Nat. Mater.*, **4** 776–81 (2005).

[23]R. E. García, B. D. Huey, and J. E. Blendell, "Virtual Piezoforce Microscopy of Polycrystalline Ferroelectric Films," *J. Appl. Phys.*, **100** [6] 064105, 10pp (2006).

[24]P. Potnis, N.-T. Tsou, and J. Huber, "A Review of Domain Modelling and Domain Imaging Techniques in Ferroelectric Crystals," *Materials (Basel)*, **4** [12] 417–47 (2011).

[25]S. Choudhury, Y. L. Li, C. E. Krill, and L. Q. Chen, "Phase-Field Simulation of Polarization Switching and Domain Evolution in Ferroelectric Polycrystals," *Acta. Mater*., **53** [20] 5313–21 (2005).
[26]S. Choudhury, Y. L. Li, C. Krill, and L. Q. Chen, "Effect of Grain Orientation and Grain Size on Ferroelectric Domain Switching and Evolution: Phase Field Simulations," *Acta Mater*., **55** [4] 1415–26 (2007).
[27]F. X. Li, X. L. Zhou, and A. K. Soh, "An Optimization-Based 'Phase Field' Model for Polycrystalline Ferroelectrics," *Appl. Phys. Lett*., **96** [15] 152905, 3pp (2010).
[28]A. Haug, J. E. Huber, P. R. Onck, and E. Van der Giessen, "Multi-Grain Analysis Versus Self-Consistent Estimates of Ferroelectric Polycrystals," *J. Mech. Phys. Solids*, **55** [3] 648–65 (2007).
[29]H. Abdolvand, M. Majkut, J. Oddershede, S. Schmidt, U. Lienert, et al., "On the Deformation Twinning of Mg AZ31B: A Three-Dimensional Synchrotron X-ray Diffraction Experiment and Crystal Plasticity Finite Element Model," *Int. J. Plast*., **70**, 77–97 (2015).
[30]H. Abdolvand, M. Majkut, J. Oddershede, J. P. Wright, and M. R. Daymond, "Study of 3-D Stress Development in Parent and Twin Pairs of a Hexagonal Close-Packed Polycrystal: Part I—*In-Situ* Three-Dimensional Synchrotron X-ray Diffraction Measurement," *Acta. Mater*., **93**, 246–55 (2015).
[31]H. Abdolvand, M. Majkut, J. Oddershede, J. P. Wright, and M. R. Daymond, "Study of 3-D Stress Development in Parent and Twin Pairs of a Hexagonal Close-Packed Polycrystal: Part II—Crystal Plasticity Finite Element Modeling," *Acta Mater*., **93**, 235–45 (2015).
[32]The Minerals Metals & Materials Society (TMS), *Modeling Across Scales: A Roadmapping Study for Connecting Materials Models and Simulations Across Length and Time Scales*. The Minerals, Metals & Materials Society, Warrendale, PA, 2015.
[33]T. Kalil and C. Wadia, *Materials Genome Initiative for Global Competitiveness*. National Science and Technology Council, Washington, DC, 2011.
[34]J. E. Daniels, A. Pramanick, and J. L. Jones, "Time-Resolved Characterization of Ferroelectrics Using High-Energy X-ray Diffraction," *IEEE Trans. Ultrason. Ferroelectr. Freq. Control*, **56** [8] 1539–45 (2009).
[35]J. C. Labiche, O. Mathon, S. Pascarelli, M. a. Newton, G. G. Ferre, et al., "Invited Article: The Fast Readout low Noise Camera as a Versatile x-ray Detector for Time Resolved Dispersive Extended x-ray Absorption Fine Structure and Diffraction Studies of Dynamic Problems in Materials Science, Chemistry, and Catalysis," *Rev. Sci. Instrum*., **78** [9] 091301, 11pp (2007).
[36]U. L. Olsen, S. Schmidt, and H. F. Poulsen, "A High-Spatial-Resolution Three-Dimensional Detector Array for 30-200 keV X-Rays Based on Structured Scintillators," *J. Synchrotron Radiat*., **15** [4] 363–70 (2008).
[37]H. O. Sørensen, S. Schmidt, J. P. Wright, G. B. M. Vaughan, S. Techert, et al., "Multigrain Crystallography," *Zeitschrift fur Krist*, **227** [1] 63–78 (2012).
[38]S. Schmidt, "GrainSpotter: A Fast and Robust Polycrystalline Indexing Algorithm," *J. Appl. Crystallogr*., **47**, 276–84 (2014).
[39]S. Schmidt, U. L. Olsen, H. F. Poulsen, H. O. Sørensen, E. M. Lauridsen, et al., "Direct Observation of 3-D Grain Growth in Al-0.1% Mn," *Scr. Mater*., **59** [5] 491–4 (2008).
[40]M. A. Groeber and M. A. Jackson, "DREAM.3D: A Digital Representation Environment for the Analysis of Microstructure in 3D," *Integr. Mater. Manuf. Innov*., **3** [1] 5, 17pp (2014).
[41]J. Oddershede, M. Majkut, Q. Cao, S. Schmidt, P. Wright, et al., "Quantitative Grain-Scale Ferroic Domain Volume Fractions and Domain Switching Strains From Three-Dimensional X-ray Diffraction Data," *J. Appl. Crystallogr*., **48**, 882–9 (2015).
[42]D. A. Hall, A. Steuwer, B. Cherdhirunkorn, P. J. Withers, and T. Mori, "Texture of Poled Tetragonal PZT Detected by Synchrotron X-ray Diffraction and Micromechanics Analysis," *Mater. Sci. Eng., A*, **409**, 206–10 (2005).
[43]L. Daniel, D. A. Hall, and P. J. Withers, "A Multiscale Model for Reversible Ferroelectric Behaviour of Polycrystalline Ceramics," *Mech. Mater*., **71**, 85–100 (2014).
[44]J. E. Daniels, J. L. Jones, and T. R. Finlayson, "Characterization of Domain Structures From Diffraction Profiles in Tetragonal Ferroelastic Ceramics," *J. Phys. D Appl. Phys*., **39** [24] 5294–9 (2006).
[45]J. K. Mackenzie, "Second Paper on Statistics Associated With the Random Distribution of Cubes," *Biometrika*, **45** [1–2] 229–40 (1958).
[46]M. Kamlah, A. C. Liskowsky, R. M. McMeeking, and H. Balke, "Finite Element Simulation of a Polycrystalline Ferroelectric Based on a Multidomain Single Crystal Switching Model," *Int. J. Solids Struct*., **42** [9–10] 2949–64 (2005).
[47]J. E. Daniels, M. Majkut, Q. Cao, S. Schmidt, J. P. Wright, and J. Oddershede, "Heterogeneous Grain-Scale Response in Ferroic Polycrystals Under Electric Field," *Sci. Rep*., **6**, 22820, 7pp (2016).
[48]Y. Tan, J. Zhang, Y. Wu, C. Wang, V. Koval, et al., "Unfolding Grain Size Effects in Barium Titanate Ferroelectric Ceramics," *Sci. Rep*., **5**, 9953, 9pp (2015).
[49]G. Arlt, D. Hennings, and G. De With, "Dielectric Properties of Fine-Grained Barium Titanate Ceramics," *J. Appl. Phys*., **58** [4] 1619–25 (1985).
[50]Y. Li, S. Y. Hu, Z. K. Liu, and L. Q. Chen, "Effect of Electrical Boundary Conditions on Ferroelectric Domain Structures in Thin Films," *Appl. Phys. Lett*., **81** [3] 427–9 (2002).
[51]A. Haug, P. R. Onck, and E. Van der Giessen, "Development of Inter- and Intragranular Stresses During Switching of Ferroelectric Polycrystals," *Int. J. Solids Struct*., **44** [6] 2066–78 (2007).
[52]K. Jayabal, A. Menzel, A. Arockiarajan, and S. M. Srinivasan, "Micromechanical Modelling of Switching Phenomena in Polycrystalline Piezoceramics: Application of a Polygonal Finite Element Approach," *Comput. Mech*., **48** [4] 421–35 (2011).
[53]Y. A. Genenko, J. Glaum, M. J. Hoffmann, and K. Albe, "Mechanisms of Aging and Fatigue in Ferroelectrics," *Mater. Sci. Eng. B Solid-State Mater. Adv. Technol*., **192** [C] 52–82 (2015).
[54]J. E. Huber, N. A. Fleck, C. M. Landis, and R. M. McMeeking, "Constitutive Model for Ferroelectric Polycrystals," *J. Mech. Phys. Solids*, **47** [8] 1663–97 (1999).
[55]A. Pathak and R. M. McMeeking, "Three-Dimensional Finite Element Simulations of Ferroelectric Polycrystals Under Electrical and Mechanical Loading," *J. Mech. Phys. Solids*, **56** [2] 663–83 (2008).
[56]P. L. Bishay and S. N. Atluri, "2D and 3D Multiphysics Voronoi Cells, Based on Radial Basis Functions, for Direct Mesoscale Numerical Simulation (DMNS) of the Switching Phenomena in Ferroelectric Polycrystalline Materials," *Comput. Mater. Contin*., **33** [1] 19–62 (2013).
[57]R. E. García, W. C. Carter, and S. A. Langer, "The Effect of Texture and Microstructure on the Macroscopic Properties of Polycrystalline Piezoelectrics: Application to Barium Titanate and PZN-PT," *J. Am. Ceram. Soc*., **88** [3] 750–7 (2005). □